

Electronic Supplementary Information

Fluorescein Sodium Ligands-Modified Silicon Nanoparticles Produce Ultrahigh Fluorescence with Robust pH- and Photo-Stability

Yiling Zhong,^{a,b} Bin Song,^a Xiaobin Shen,^a Daoxia Guo,^a and Yao He^{,a}*

^aJiangsu Key Laboratory for Carbon-Based Functional Materials and Devices, Institute of Functional Nano & Soft Materials (FUNSOM), and Collaborative Innovation Centre of Suzhou Nano Science and Technology (NANO-CIC), Soochow University, Suzhou, Jiangsu 215123, China

E-mail: yaohe@suda.edu.cn

^bSchool of Chemistry, University of New South Wales, Sydney, NSW, 2052, Australia

Table of Contents

Experimental methods	S4-10
Schematic illustration of a proposed synthesis mechanism	S11
SiNPs of different sizes and their size-independent PL	S12
TEM images of the SiNPs without FS ligands (i.e., blue (a) and (b) orange SiNPs)	S13
TEM image of the control group (~3.8 nm SiNPs), and the normalized PL spectra of the green SiNPs and the control group	S14
The EDX pattern of the SiNPs	S15
TGA profiles of SiNPs and FS	S16
FTIR spectra of APS, FS, and SiNPs	S17-18
¹ H NMR spectrum of FS, FS after treatment of microwave irradiation, and SiNPs	S19-20
PLQY measurements of the SiNPs	S21
Photostability comparison of FS and SiNPs	S22-23
Temporal evolution of fluorescence intensity of FS (after microwave reaction) and SiO ₂ @FS aqueous sample solution under various pH values	S24
Cell viability of cells incubated with the SiNPs for different time	S25
Fluorescence decays of fluorescein sodium (FS) and the as-prepared SiNPs	S26
Comparison dialysis processes of SiNPs and FS	S27
Photographs of the APS (after microwave reaction) under ambient light (left) and 365 nm irradiation (right)	S28
Fluorescent properties of FITC (after microwave reaction)	S29
TEM images of the SiO ₂	S30
TEM image of SiO ₂ with small size of ~20 nm and photographs of SiO ₂ @FS (~20 nm SiO ₂) sample under ambient light or 365 nm irradiation	S31
A comparison chart of different synthesis methods	S32

Video S1 shows the fluorescence signals change of the FS and SiNPs samples with the addition of HCl. As shown in Video S1, 1 mL HCl is dropped into the aqueous solution of FS and SiNPs, respectively. While the two samples exhibit distinct fluorescence in the initial state, the fluorescent signals of FS are gradually reduced with increasing amount of HCl. Specifically, the fluorescence of FS completely disappears after adding HCl with a total volume of 1 mL. In remarkable contrast, the SiNPs sample preserves stable and bright fluorescence under the same experiment conditions, indicating the robust pH stability of the resultant SiNPs.

Experimental methods

Materials and Devices. (3-Aminopropyl)trimethoxysilane (97%) was purchased from Sigma-Aldrich. Fluorescein sodium ($C_{20}H_{10}Na_2O_5$) was purchased from Sinopharm Chemical Reagent Co., Ltd (China). All chemicals were used without additional purification. All solutions were prepared using Milli-Q water (Millipore) as the solvent. The microwave system NOVA used for synthesizing SiNPs was made by Preekem of Shanghai, China. The system operates at 2450 MHz frequency and works at 0-500 W power. Exclusive vitreous vessels with a volume of 15 or 30 mL are equipped for the system to provide security during reactions demanding high temperature and pressure. In addition, the microwave system Anton Paar Monowave 300 used for synthesizing silicon nanomaterials was made by Anton Paar, United States. Exclusive vitreous vessels with a volume of 10 or 30 mL are equipped for the system to provide security during reaction demanding high temperature and pressure. The SiNPs were characterized by UV-vis absorption, photoluminescence (PL), transmission electron microscopy (TEM), and high-resolution TEM (HRTEM), nuclear magnetic resonance (NMR) spectroscopy, thermogravimetric analysis (TGA) and Fourier-transform infrared (FTIR) spectroscopy. Optical measurements were performed at room temperature under ambient air conditions. UV-vis absorption spectra were recorded with a Perkin-Elmer lambda 750 UV-vis near-infrared spectrophotometer. PL measurements were performed using a HORIBA JOBIN YVON FLUOROMAX-4 spectrofluorimeter. The photoluminescence quantum yield (PLQY) of samples was estimated using fluorescein sodium in 0.01 M NaOH (PLQY: 93%) or quinine sulfate in 0.1 M H_2SO_4 (PLQY: 58%) as a reference standard, which was freshly prepared to reduce the measurement error. TEM and HRTEM samples were prepared by dispersing the sample onto carbon-coated copper grids with the excess solvent evaporated. The TEM/HRTEM overview images were recorded using the FEI Tecnai F20 transmission electron microscope equipped with an energy dispersive spectroscopy at an acceleration voltage of 200 kV. Dynamic Light Scattering (DLS) was made by Malvern Corp,

U.K. (ZEN 3690). 1 mL SiNPs sample was transferred into an exclusive vitreous vessel for DLS measurements. Experiment parameters were as follows: 0.8872 Cp; RI: 1.330; and dielectric constant: 78.5. Energy-dispersive X-ray (EDX) spectroscopy was utilized to determine the composition of the resultant SiNPs. The SiNPs samples were first dispersed onto carbon-coated copper grids with the excess solvent evaporated and then characterized by using the FEI Tecnai F20 transmission electron microscope equipped with an energy dispersive spectroscope at an acceleration voltage of 200 kV. Ultra-High Intensity UV-A Lamp (MAXIMA™ ML-3500S/FA, 365 nm) was made by SPECTRONICS, USA. The Ultra-High Intensity UV-A Lamp with a spot reflector has a nominal steady-state UV-A intensity of 50,000 $\mu\text{W}/\text{cm}^2$ at 15 inches (38 cm).

Synthesis of SiNPs. The SiNPs precursor solution was prepared by adding 100 mL of (3-aminopropyl)trimethoxysilane to 400 mL aqueous solution dispersed with 0.1 g of fluorescein sodium (FS). The mixture was stirred for 20 min. The resultant precursor solution was transferred into the exclusive vitreous vessel with a volume of 30 mL for microwave reaction (e.g., 180 °C/60 min, 180 °C/ 2 h and 200 °C/ 3h). After microwave irradiation, the SiNPs sample was removed and the temperature cooled to < 30 °C naturally. Afterward, the SiNPs sample was further purified by dialysis (MWCO: 500, Viskase). The purified SiNPs aqueous solution with strong green luminescence was used for the investigation of physical/chemical/optical properties, and cytotoxicity assessment. In order to obtain SiNPs with larger sizes, the reaction time was prolonged, or the reaction temperature was increased to some extent with all other the experimental procedures kept the same. Microwave dielectric heating was utilized in our method to take advantage of its three dominant merits, such as rapid temperature elevation, homogeneous heating, and high reaction selectivity.

The SiNPs without FS ligands (i.e., blue, green and orange SiNPs) were prepared based on previously reported methods¹:

Blue SiNPs^{1a}: The SiNPs precursor solution was prepared by adding 100 mL of (3-aminopropyl)trimethoxysilane to 400 mL N₂-saturated aqueous solution dispersed with 18.6 g of trisodium citrate dihydrate. The mixture was stirred for 10 min. The resultant precursor solution was transferred into the exclusive vitreous vessel with a volume of 30 mL. The blue SiNPs were prepared under 160 °C/15 min.

Green SiNPs^{1b}: The green SiNPs without FS ligands precursor solution was prepared by adding 100 mL of (3-Aminopropyl)trimethoxysilane to 400 mL aqueous solution dispersed with 18.6 g of trisodium citrate dihydrate. And then a certain amount of HCl (3 M) was added into the mixture solution to obtain the desired pH (pH = ~ 4). The pH value was monitored by Seven Multi pH meter (Mettler Toledo). The resultant precursor solution was transferred into the exclusive vitreous vessel with a volume of 30 mL. The green SiNPs without FS ligands were prepared under 180 °C/60 min.

After microwave irradiation, the SiNPs samples were removed when the temperature cooled to < 30 °C naturally. The SiNPs were purified by dialysis.

Orange SiNPs^{1c}: The orange SiNPs precursor solution was prepared by adding 10 mL of (3-Aminopropyl)trimethoxysilane (concentration: 1.027 g/mL) to 10 mL Cy7 aqueous solution (concentration : 50 µg/mL) in a common glass bottle with volume of 60 mL. The orange SiNPs were readily achieved in ~60 min via one-step reaction at room temperature (20-25 °C) and atmospheric pressure. The as-prepared orange SiNPs were purified by dialysis.

Synthesis of FS (after microwave reaction). 0.02 g FS was dispersed in 100 ml Milli-Q water as precursor solution. And then the precursor solution was poured into the exclusive vitreous vessel with a volume of 30 mL for further microwave reaction. The reaction condition was the same as that of SiNPs.

Synthesis of SiO₂. SiO₂ nanoparticles were prepared by Stöber method.² Typically, first, 1.2 mL of ammonia was added into 250 ml of ethanol under stirring and kept for 5 min. Then, 20 mL of TEOS was added dropwise. After stirring for 24 h at room temperature, the solution was centrifuged and washed three times with ethanol and water. Finally, SiO₂ nanoparticles were dried at 60 °C in a vacuum drying oven overnight. To prepare amino-modified SiO₂ nanoparticles, 8 mL of 1 wt% SiO₂ solution and 0.2 mL of APTES were added into 20 mL of isopropanol and ultrasonicated for 30 min. The solution was heated to 60 °C and stirred for 6 h, eventually producing SiO₂-NH₂ nanoparticles. To exclude impurities influence, the residual reagents were removed by centrifuging and washing several times. The purified SiO₂ nanoparticles were dried at 60 °C in a vacuum drying oven overnight. The TEM images of the resultant SiO₂ were shown in Fig. S15.

The ~20 nm SiO₂ were synthesized based on a previous report.^{2b} In brief, 0.06 mmol of hexadecyltrimethylammonium bromide (CTAB) and 2 ml of 0.02 M ammonium hydroxide aqueous solution were added into 8 ml Milli-Q water. Then the solution was stirred at 30 °C for ~30 min until CTAB fully dissolved. After that, 0.11mmol TEOS was added into the solution under vigorous stirring and the solution was further stirred at 30 °C for 24 h. Afterwards, the solution was cooled to room temperature and then transferred into a dialysis membrane tube. The solution in the dialysis tube was dialyzed in the mixture solution including Milli-Q water, ethanol and acetic acid (the volume ratio 1:1:0.007) to extract CTAB. This process was repeated several times. The solution was then dialyzed in Milli-Q water for ~48 h. The purified sample was then collected and dried.

Synthesis of SiO₂@FS. For the preparation of SiO₂@FS, 0.5 g of SiO₂ was added into to 100 ml aqueous solution dispersed 0.02 g of FS and stirred for 10 min. Afterward, the precursor solution was transferred into the vitreous vessel. The vessel was put into the microwave reactor and reacted under 180 °C/60 min to produce SiO₂@FS.

Nuclear magnetic resonance (NMR) spectroscopy. To show the reaction-induced chemical bonding, 20 mg of SiNPs was dispersed in 600 μl D_2O . ^1H NMR spectrum were recorded on 400 MHz Bruker spectrometers, and D_2O served as internal standard in the characterization.

Photostability comparison of FS and SiNPs. To guarantee reliable comparison, the PL intensity of FS and SiNPs was adjusted to the same value. The two samples were continuously irradiated for different time intervals using an ultrahigh intensity UV-A lamp (MAXIMATM ML-3500S/FA, 365 nm). The distance between the UV-A lamp and the samples is 10 cm.

pH stability of SiNPs. The pH of the SiNPs aqueous solution was varied by dropwise addition of HCl (1 mol/L) or NaOH (1 mol/L). The pH value was monitored by Seven Multi pH meter (Mettler Toledo), while concurrently the PL intensity of the samples was recorded by the HORIBA JOBIN YVON FLUOROMAX-4 spectrofluorimeter.

Synthesis of FITC (after microwave reaction). 0.02 g FITC was dispersed in 100 ml Milli-Q water as precursor solution. And then the precursor solution was poured into the exclusive vitreous vessel with a volume of 30 mL for further microwave reaction. The reaction condition was the same as that of SiNPs.

Photoluminescence quantum yield (PLQY) measurements. According to the different maximum emission wavelengths of the as-prepared SiNPs and control SiNPs, the PLQY of samples was estimated using FS in 0.01 M NaOH (QY = 93%) or quinine sulfate in 0.1M H_2SO_4 (literature quantum yield: 58%) as a reference standard, which was freshly prepared to reduce the measurement error,²⁻¹¹ respectively. In detail, the PL spectra of a given sample of the nanoparticles in aqueous solution and an organic dye, whose PL spectrum overlaps

significantly with that of the nanoparticles sample, were measured under the same setting as that of HORIBA JOBIN YVON FLUOROMAX-4 spectrofluorimeter. The optical densities (OD) at the excitation wavelength of the dye and the nanoparticles sample were set to identical values. The OD at either the first exciton absorption peak of the nanocrystals or the main absorption peak of the dye was below 0.1 in order to avoid any significant reabsorption. The integrated PL intensities (via areas) of the nanoparticles and dye were calculated from the fully corrected fluorescence spectrum. To reduce the measurement error as much as possible, more than six different solution concentrations of nanoparticles and the corresponding dye were used in the measurement. The integrated PL intensities vs corresponding absorbance were plotted. The plots yielded two straight lines. The gradients of the straight lines were then used to determine the PLQY according to the following equation:

$$Q_x = Q_r (M_x / M_r) (n_x / n_r)^2.$$

Where n is the average refractive index of the solvent, M is the gradient of straight line, Q is quantum yield, and subscripts x and r refer to the test samples and reference solutions, respectively. In addition, the wavelength of excitonic absorption peak of the nanoparticles was set as the excitation wavelength for measurement.

Thermogravimetric analysis. TGA was performed using a METTLER TOLEDO TGA/STDA 851 instrument. The samples, which ranged in weight from 5 to 12 mg, were placed in a porcelain crucible and heated under air atmosphere from 30 to 800 °C at a rate of 10 °C/min.

MTT assay of cell viability. Cells (e.g., HeLa cells, and human retinal pigment epithelial cell line (ARPE-19) were dispersed in 96-well plates (90 μ L in each well containing 1×10^4 cells per well). Different concentrations (0.5, 1, 2, 4, 8, 16, 32, 64, and 128 μ g/mL) of SiNPs

solution were added to each well and incubated for 24 and 48 h in a humidified atmosphere at 37 °C with 5% CO₂. The cytotoxicity of the SiNPs was evaluated by the MTT (3-(4,5-dimethylthiazol-2-yl)-2,5-diphenyltetrazolium bromide) assay (thiazolyl blue tetrazolium bromide (M5655)). The assay was based on the accumulation of dark-blue formazan crystals inside living cells after exposure to MTT, which is a well-established protocol for assessment of cellular viability. Destruction of cell membranes by the addition of sodium dodecylsulfate resulted in the liberation and solubilization of crystals. The number of viable cells was thus directly proportional to the level of the initial formazan product created. The formazan concentration was finally quantified using a spectrophotometer by measuring the absorbance at 570 nm (ELISA reader). A linear relationship between cell number and optical density was established, thus allowing for accurate quantification of changes in the rate of cell proliferation. To ensure reproducibility, three independent experiments were performed, and all measurements were carried out in triplicate.

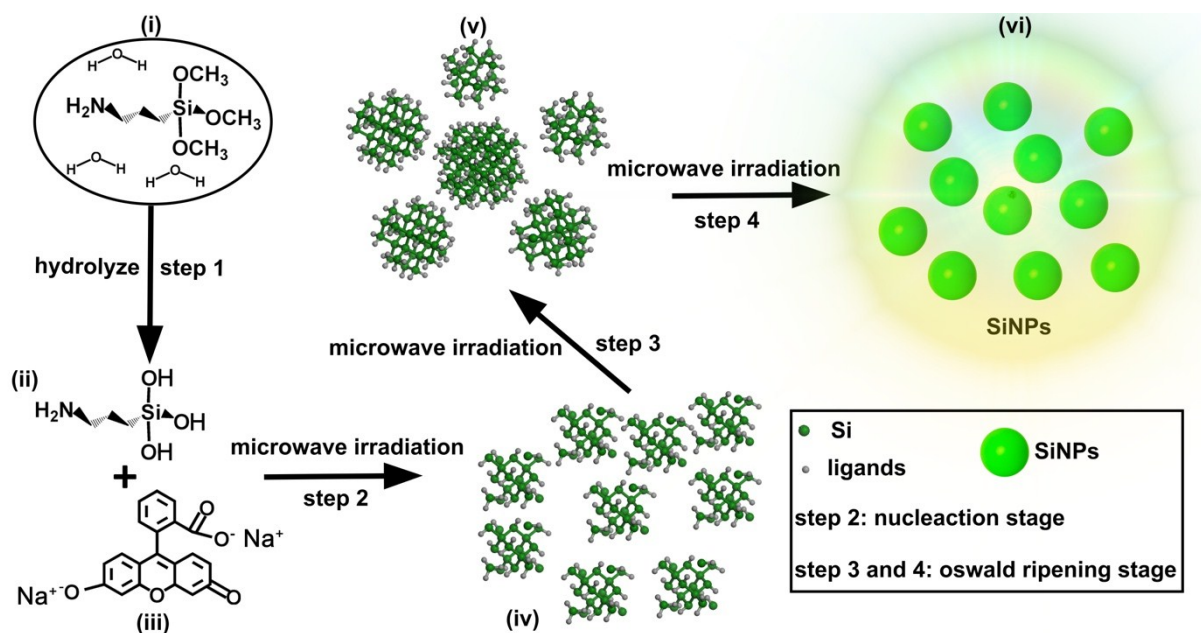


Fig. S1 Schematic illustration of a proposed synthesis mechanism. Typically, (3-Aminopropyl)trimethoxysilane (i) is first hydrolyzed to produce (3-Aminopropyl)trihydroxysilane (ii) through established hydrolysis reaction in aqueous phase in the first step (step 1).^{1a,b,6} Afterwards, (3-Aminopropyl)trihydroxysilane molecules are reduced by FS ((iii), severed as reductant and ligands) under microwave irradiation to produce crystal nuclei (iv) in the second step (step 2). When sufficient crystal nuclei are formed, the Ostwald ripening stage is triggered in the following reaction steps (step 3 and 4). Typically, small-size nanocrystals are first formed in the initial Ostwald ripening stage (step 3: (iv)→(v)). With further reaction, nanocrystal growth continues at the expense of dissolution unstable nanocrystals with small sizes, eventually producing more stable and larger-size SiNPs in the fourth step (step 4: (v)-(vi)).

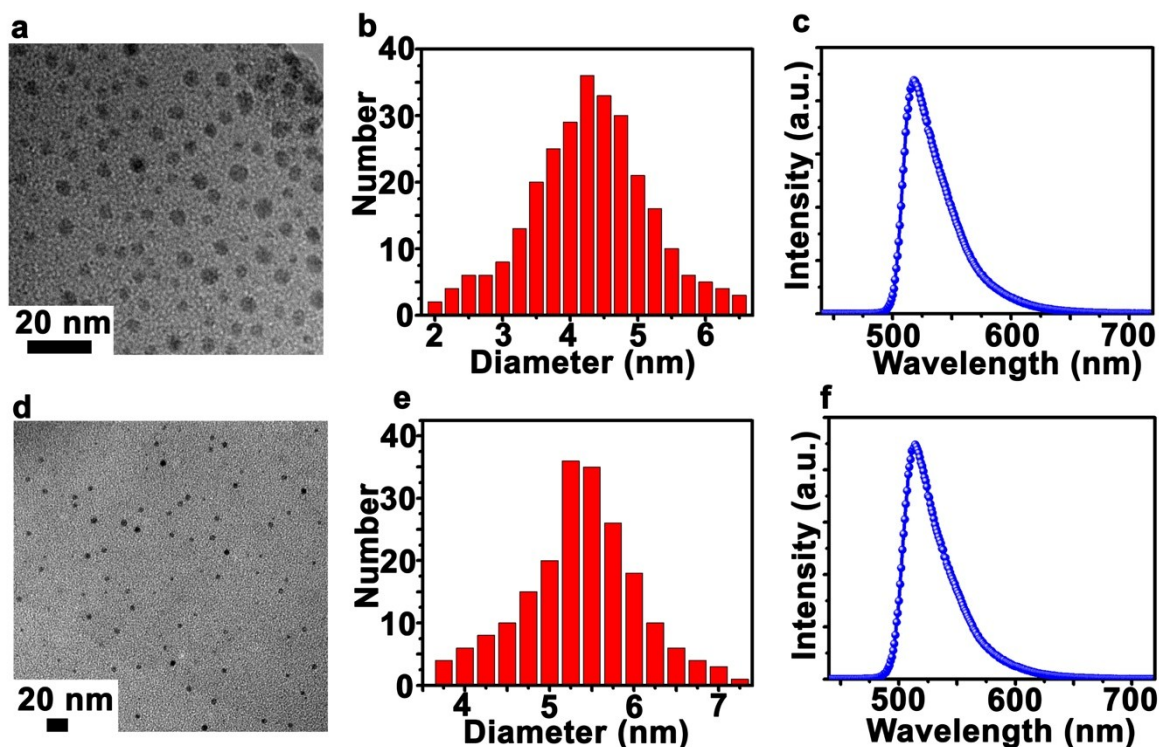


Fig. S2 (a-c) TEM image, size distribution and PL spectra of the SiNPs with an average diameter of ~ 4.2 nm. (d-f) TEM image, size distribution and PL spectra of the SiNPs with an average diameter of ~ 5.3 nm. As shown in Fig. S2, the SiNPs with different sizes (e.g., ~ 4.2 and 5.3 nm) are prepared by controlling the experimental conditions (e.g., reaction time and temperature: 180 °C/ 2 h and 200 °C/ 3 h, respectively). The PL peaks of the SiNPs with different sizes (e.g., ~ 3.7 , 4.2 and 5.3 nm) are almost the same, locating at ~ 515 nm. In addition, the SiNPs with different sizes feature narrow emission spectral width (full width at half-maximum (fwhm): ~ 50 nm). These experimental results suggest that the ultrabright PL from the SiNPs is largely dependent to the surface ligands but not the particle size, which is similar to previously reported SiNPs.¹²⁻¹⁴

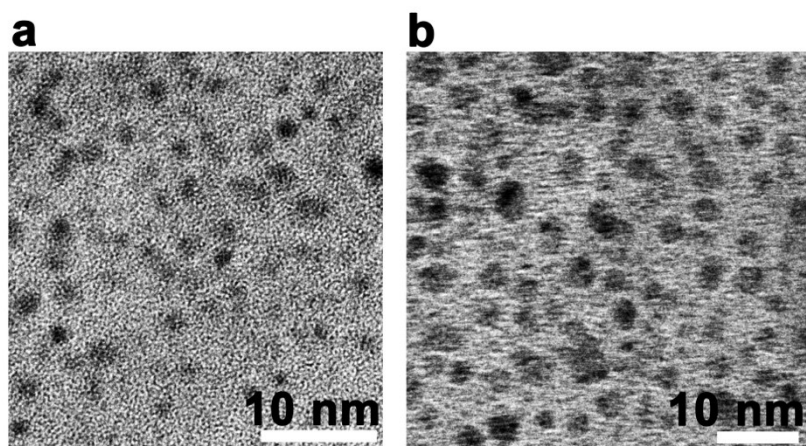


Fig. S3 TEM images of the SiNPs without FS ligands (i.e., blue (a) and (b) orange SiNPs).

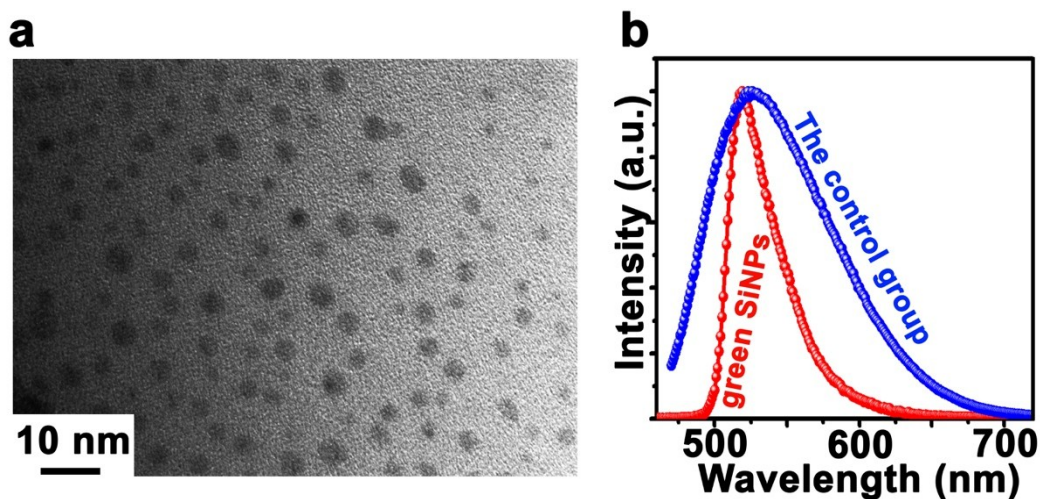


Fig. S4 (a) TEM image of the control group (i.e., ~ 3.8 nm SiNPs, green SiNPs without FS ligands). (b) The normalized PL spectra of the green SiNPs with FS ligands (red line) and the control group (i.e., ~ 3.8 nm SiNPs, green SiNPs without FS ligands, blue line) (excitation wavelength: 450 nm). The ~ 3.8 nm SiNPs, served as the control group, are prepared based on our previous reports (quantum yield efficiency: $\sim 20\%$).^{1b} Fig. S4a displays the TEM image of the control group, in which the SiNPs appear as spherical particles with good monodispersity. The control group possesses almost the same size as the green SiNPs (~ 3.7 nm). As shown in Fig. S4b, the green SiNPs and the control group exhibit similar maximum emission wavelength with excitation at 450 nm (the maximum emission wavelength of the green SiNPs and the control group are ~ 515 and 522 nm, respectively), while the full width at half-maximum (fwhm) of the control group is broader ~ 50 nm than that of the green SiNPs (the fwhm values of the green SiNPs and the control group are ~ 50 and 100 nm, respectively). In comparison to the control group, the green SiNPs feature strong fluorescence and narrow emission spectral width (fwhm, ~ 50 nm), which should be attributable to the effect of the surface ligands. The surface ligands (i.e., FS) can form a strong surface effect with a uniform surface center, largely dominating the light-emitting process of the green SiNPs, which is similar to previously reported SiNPs.¹⁴

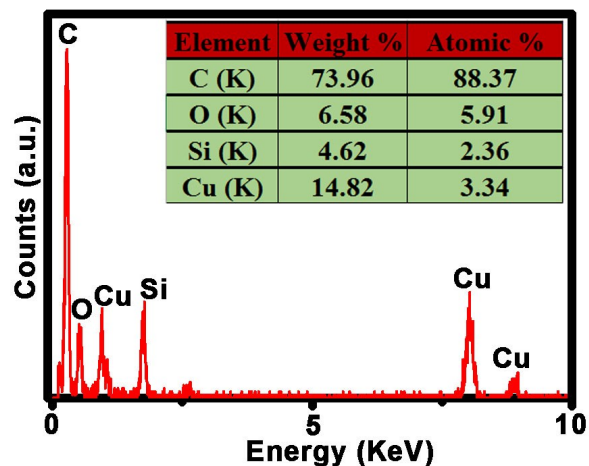


Fig. S5 EDX pattern of the SiNPs samples. Inset table presents the corresponding elemental ratio (weight and atom percentage) calculated by the EDX software (K-shell intensity ratios are indicated). The EDX pattern qualitatively demonstrates the existence of Si and O in the SiNPs. Nevertheless, it is worthwhile to point out that, for EDX measurement, a quantitative analysis of elemental ratios is not possible since the supporting substrate (e.g., carbon-coated copper grids) was carbon containing a measurable amount of residual oxygen. Therefore, the element weight concentrations listed in the table are not reliable.^{1,5,9}

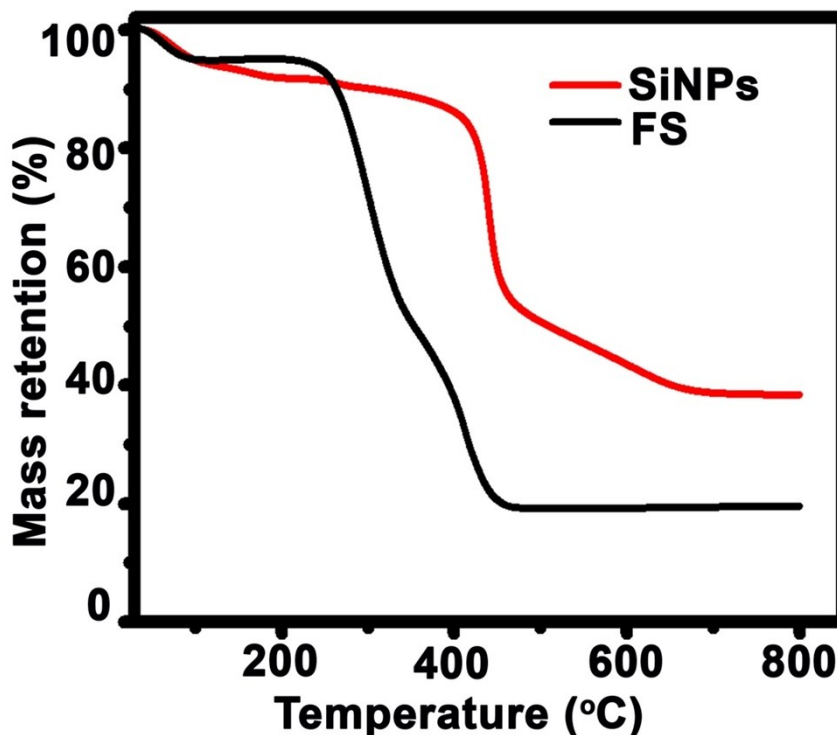


Fig. S6 TGA profiles of SiNPs (red line) and FS (black line). The experiments are run at heating rate of 10 °C/min under air. To estimate the coverage rate of the organic surface ligands of the as-prepared SiNPs, TGA characterization is further performed. TGA is carried out under a flow of air with an increase in temperature ranging from 30 °C to 800 °C. As shown in Fig. S6, TGA of SiNPs (red line) shows a typical three-stage mass loss in air: (i) mass loss below 100 °C, which is attributed to water loss; (ii) mass loss around 400 °C, which is due to the burning of surface organic ligands (containing carbon, oxygen, and hydrogen); and (iii) mass loss between 480-680 °C, corresponding to the further burning of carbonous residues. In air, rapid mass loss between 240 and 460 °C is observed for the FS (black line), which is ascribed to the burning of carbon compounds. The TGA results indicate that the inorganic residues are produced (such as silicon oxide (red line, the SiNPs sample) and sodium oxide (black line, the FS sample)), because the organic residue should be burn at this experimental condition. At 800 °C, the residual weight percentages of FS and SiNPs are 19.6% and 38.4 %, respectively.¹⁵⁻¹⁹

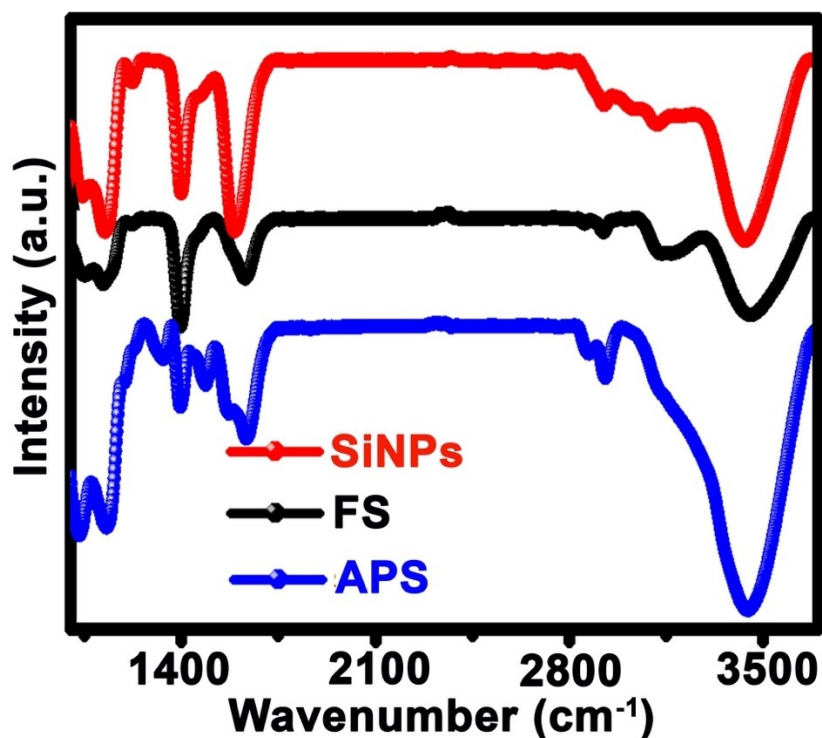


Fig. S7 FTIR spectra of APS, FS, and SiNPs, exhibiting distinct absorption peaks at 1000-3700 cm^{-1} .

Furthermore, FTIR spectra of the resultant SiNPs, FS, and APS are measured in our case, exhibiting several distinct absorption peaks at 1000-3700 cm^{-1} (Fig. S7). Typically, for FS (black line), the strong FTIR absorbance peaks at 1115, 1215, 1393, 1573, 3100 cm^{-1} are ascribed to the vibrational of aromatic C-H in plane bend bond, C-O-C stretching vibration of the xanthene ring, aromatic skeletal C-C stretching vibration, the xanthene ring skeletal C-C stretch containing conjugated carbonyl band and asymmetric carboxylate stretching vibration, and C-H stretching vibration of aromatic, respectively. And the broad band (3300-3500 cm^{-1}) can be attributed to absorbed water.²⁰⁻²² For APS, the sharp absorbance peak at ~1060, 1390-1440, 1580, 2850-2950, and 3400 cm^{-1} are assigned to the vibrational stretch of Si-O bonding, C-O vibration, N-H bending vibrations, C-H stretching vibration of alkane, and the N-H stretching vibration, respectively.^{1,6} The characteristic FTIR peaks of the as-prepared SiNPs, which are synthesized by using APS and FS as reaction precursors, located at 1060, 1115,

1215, 1393, 1580, 1600-1680, 2850-3200, 3300-3500 cm^{-1} are assigned to the vibrational stretch of Si-O bonding, the vibrational of aromatic C-H in plane bend bond, C-O-C stretching vibration of the xanthene ring, aromatic skeletal C-C stretching vibration, C-C stretching vibration of the xanthene ring, C=O stretching vibration, alkane and aromatic C-H stretching vibration, and absorbed water, respectively (red line). The FTIR results further demonstrate that FS are attached on the SiNPs as ligands.

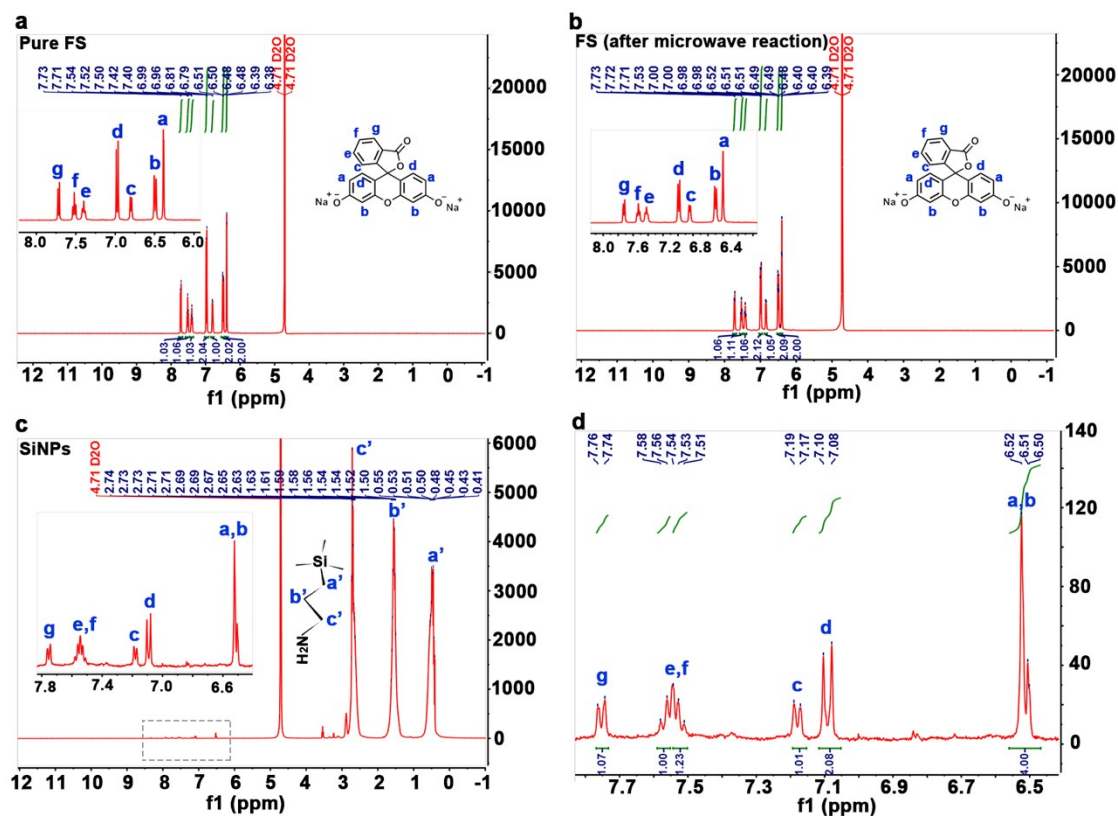


Fig. S8 ¹H NMR spectrum of (a) FS, (b) FS after treatment of microwave irradiation, (c) SiNPs, and (d) enlarged the detail spectrum of SiNPs in the range of 6.5-7.8 ppm.

Fig. S8a displays the well-resolved and sharp NMR peaks for the pure FS molecule, and those labelled a-g represent the standard positions for each proton in the pure FS molecule, respectively. After 180 °C/1h treatment with microwave irradiation (Fig. S8b), the proton chemical shifts, spin-spin splitting, and integrated proton numbers, remain almost the same as that of the pure FS, indicating that the molecular structure of FS cannot be easily broken under microwave irradiation. Furthermore, these results also show that the self-polymerization of FS molecules haven't happened under this experimental condition. In addition, ¹H NMR spectrum of the SiNPs (Fig. S8c) shows significant proton signals of segmental structure of APS from 0.4-2.7 ppm. Moreover, the characteristic peaks of neat FS molecule can also be observed in the corresponding SiNPs but with a dramatic broadening of NMR peaks (Fig. S7c and d), especially for the peaks labelled a and b, e and f at 6.52 ppm

and 7.54 ppm. These results demonstrate that the FS molecules are indeed attached on the surface of the resultant SiNPs and the peak broadening is caused by the restricted tumbling of surface-bound ligands compared to their free state.²³⁻²⁵ It also should be noted that after the fluorescein molecules as ligands of SiNPs, the chemical shift of proton labelled as c will migrate to the low field (from 6.8 to 7.18 ppm) due to deshielding effect, demonstrating that the attachment will decrease the electron cloud density of fluorescein molecules. Utilizing ¹H NMR profiles to estimate surface coverage is difficult in our case, because the proton signal from internal standard (TMS) cannot be observed in D₂O environment.

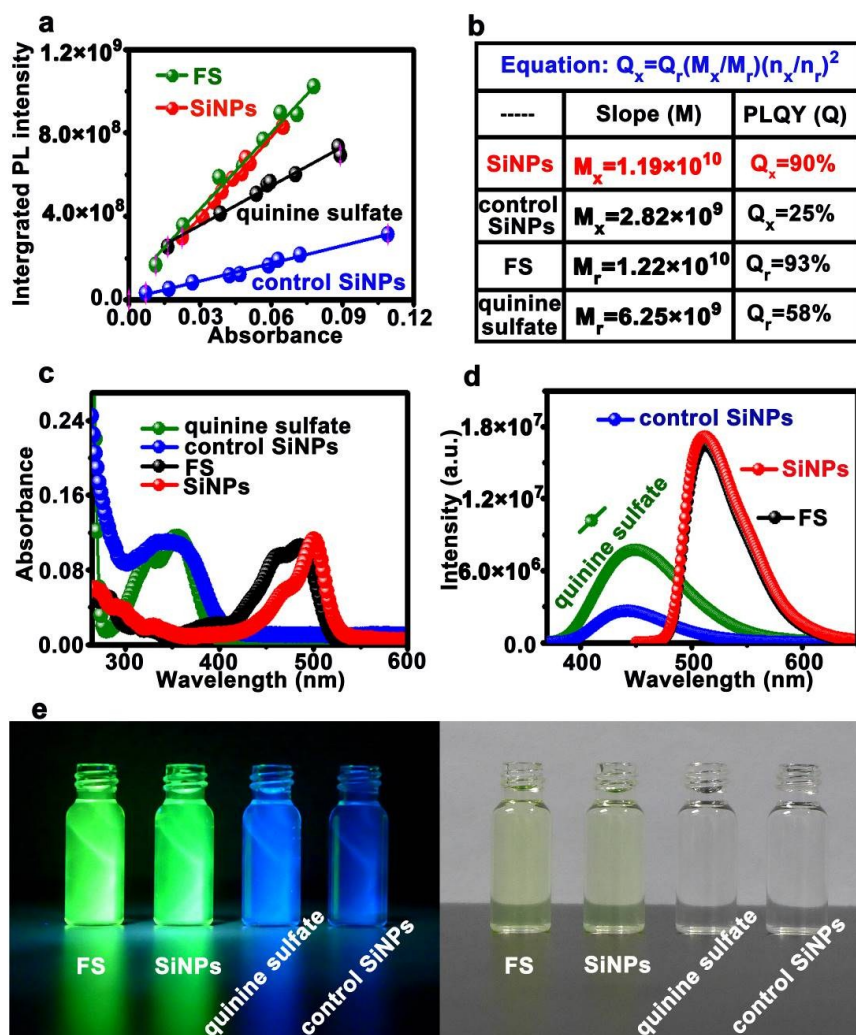


Fig. S9 (a) A typical example of integrated PL intensity dependence on the absorbance for the as-prepared SiNPs (red line), FS (green line), control SiNPs (blue line) and quinine sulfate (black line) in 0.1 M H₂SO₄. The solid lines represent the fitting results for each set of data. (b) PLQYs of the samples were calculated by using the equation: $Q_x = Q_r (M_x/M_r) (n_x/n_r)^2$. Absorption (c) and photoluminescence (d) spectra of the as-prepared SiNPs, FS, control SiNPs and quinine sulfate. (e) Photographs of the as-prepared SiNPs, FS, control SiNPs and quinine sulfate solution under 365 nm irradiation (left) or ambient light (right).

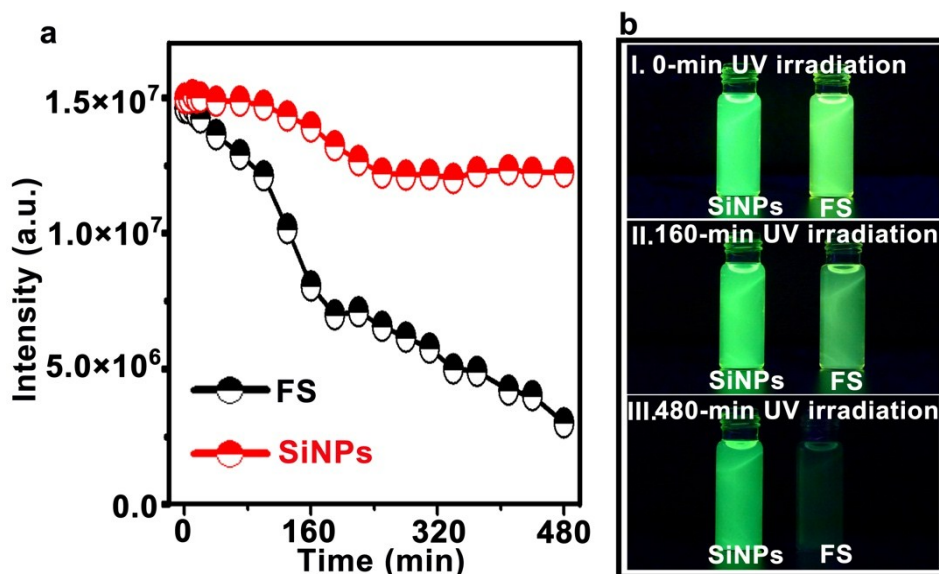


Fig. S10 (a) Photostability comparison of FS and SiNPs. (b) Photographs of FS and SiNPs aqueous solution under UV irradiation for different time. All samples are continuously irradiated by a UV lamp (MAXIMATM ML-3500S/FA, 365 nm).

We further compare the optical performance of the samples exposed under long-time (e.g., 480 min) UV treatment, because UV radiation is known to induce photobleaching of fluorescent organic dyes.^{26,27} In our experiment, FS is used as the control group. The FS sample shows approximately 50% of the original PL intensity after 160 min of UV irradiation, and very weak fluorescence after 480-min irradiation due to severe photobleaching (Fig. S10a, black line). In sharp contrast, the fluorescence intensity of SiNPs decreases only slightly, preserving approximately 85% of the initial intensity after 480 min of UV irradiation (Fig. S10a, red line). Corresponding photographs of the two samples treated by UV irradiation with different time period are shown in Fig. S10b. The fluorescence of the FS sample is distinct in the beginning of UV irradiation (Fig. S10b (I)), but gradually vanishes as irradiation time increases (Fig. S10b (II)), becoming negligible after 480 min of UV irradiation (Fig. S10b (III)) due to high-intensity UV-induced destruction of organic molecular structure.^{1,3-6,28-34} In contrast, the SiNPs sample preserves stable and bright fluorescence during long-time (e.g.,

480 min) irradiation under the same experiment conditions (Fig. S10b (III)). These results provide convincing demonstration of the superior photostability of the SiNPs compared to FS.

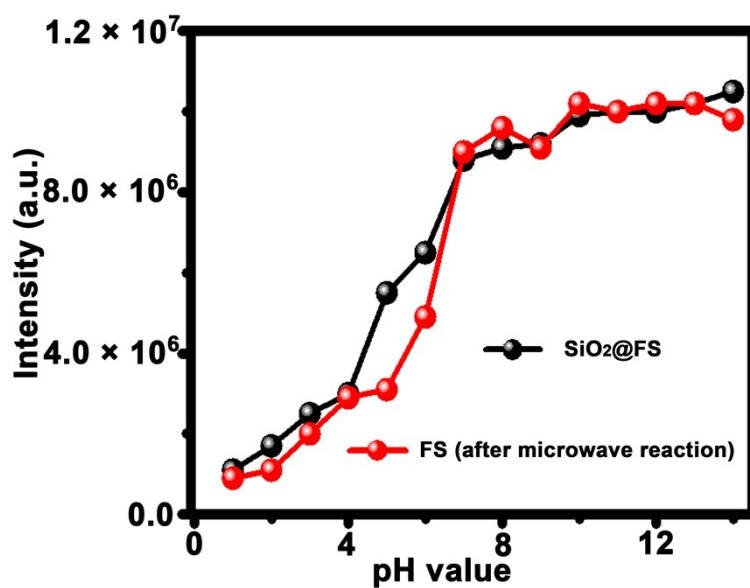


Fig. S11 Temporal evolution of fluorescence intensity of FS (after microwave reaction) and $\text{SiO}_2@FS$ aqueous sample solution under various pH values. Fig. S11 shows that PL intensity of both FS (after microwave reaction) and $\text{SiO}_2@FS$ samples dramatically decrease from basic to acidic environments in the pH range of 1-14.

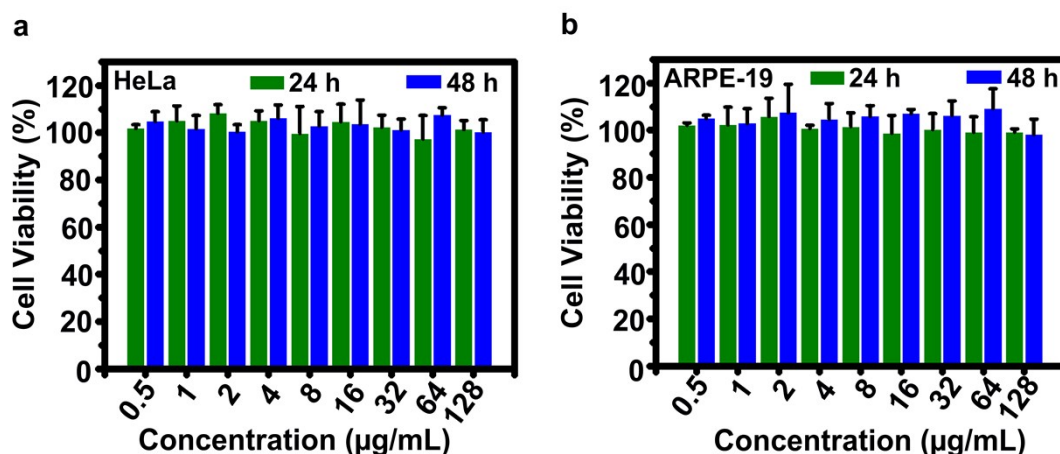


Fig. S12 Cytotoxicity assessment of the as-prepared SiNPs. Cell viability of HeLa cells (a), and human retinal pigment epithelial cell line (ARPE-19) (b) incubated with the SiNPs for 24 and 48 h, respectively. The cell viability is calculated as the percentage from the viability of the control (untreated) cells. The viability of the control cells is considered 100%. The results are the means \pm SD from three independent experiments.

In vitro toxicity of different concentration (0.5, 1, 2, 4, 8, 16, 32, 64, 128 $\mu\text{g/mL}$) of the resultant SiNPs is investigated using established MTT assay. Fig. S12 shows that the cell viabilities of cancer cells (i.e., HeLa cells) and normal cells (i.e., ARPE-19) both maintain above 90% during 48-h incubation with SiNPs, whose concentration ranges from 0.5 $\mu\text{g/mL}$ to 128 $\mu\text{g/mL}$. These data suggest feeble cytotoxicity of the SiNPs, which is due to favorable biocompatibility of silicon and well consistent with previous reports.^{1,3-6}

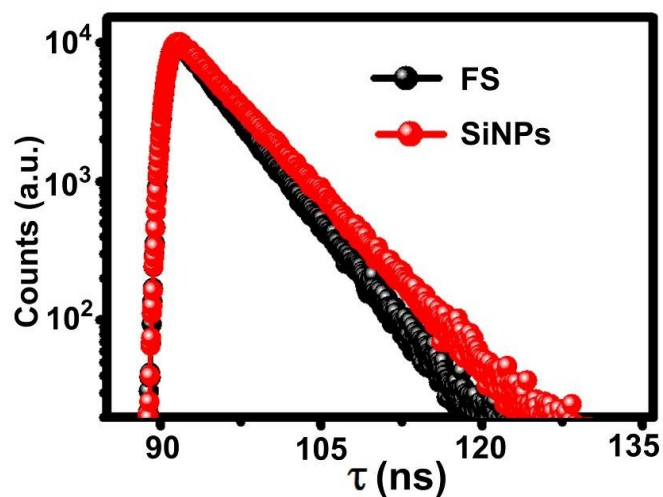


Fig. S13 Fluorescence decays of FS and the as-prepared SiNPs. PL decay of FS and the resultant SiNPs is determined, as displayed in Fig. S13. Typically, the PL decay curves of FS and SiNPs are well fit to second-order exponential decay. The decay times of components of FS are 3.015 and 4.464 ns, respectively, with a calculated average lifetime of 4.36 ns. The fluorescent lifetime of the as-prepared SiNPs also extremely short, ranging at nanosecond level (i.e. the decay times of components are 2.547, and 5.228 ns, respectively, with a calculated average lifetime of 5.18 ns). SiNPs and FS exhibit similar fluorescence lifetime. The possible reason for this is that fluorescein molecules as ligands are attached on the SiNPs, which have been confirmed by a series of physical/chemical characterizations of SiNPs. Many previous reports prove that the surface chemistry of SiNPs plays a key role in determining many of their properties.^{12-14,35} Therefore, the fluorescence lifetime of SiNPs surface-covered by FS is affected by surface ligands. However, optical performance of the SiNPs is superior to that of FS (such as photostability, pH-stability, etc.), which distinguish fluorescence of the SiNPs from that of FS. Additionally, the short lifetime of the SiNPs is in marked contrast to long fluorescent lifetime (tens of microseconds to milliseconds) of bulk silicon featuring distinct indirect band gap.³⁶⁻³⁸ These data indicate the SiNPs belong to “direct bandgap-like” materials with fast recombination, as thus, are able to produce the strong fluorescence, as observed in Fig. 2.

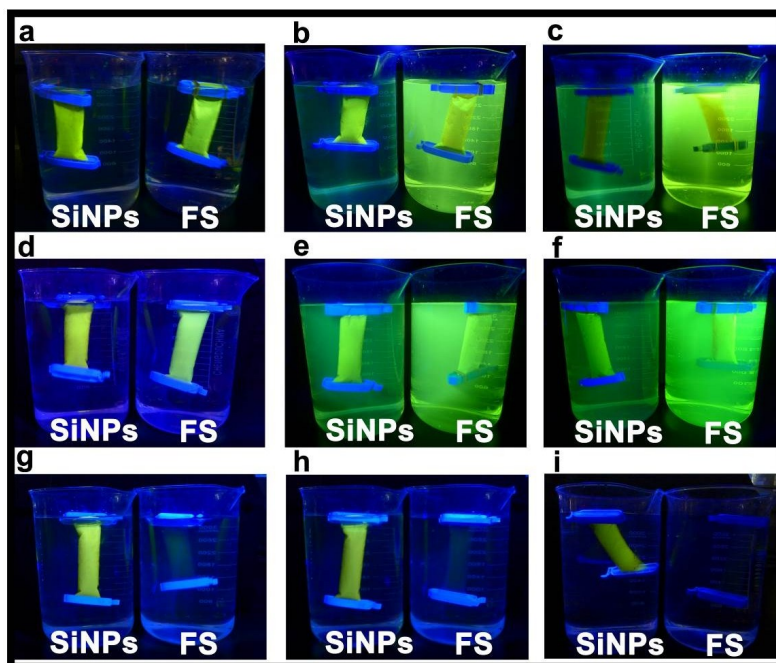


Fig. S14 Dialysis processes of SiNPs and FS sample. (a-i) show photographs of the SiNPs and FS samples under UV irradiation at different dialysis period. The two samples exhibit distinct fluorescence during initial dialysis (a). However, FS molecules are gradually filtrated with increasing dialysis treatment time (e.g., 0.5 h (b), and 2 h (c)). Meanwhile, the residual FS molecules in the SiNPs aqueous solution are also removed by dialysis (MWCO: 500, Viskase). And then the water is exchanged after 2-h dialysis (d). FS molecules are gradually filtrated (e and f) once again. The above steps are repeated for several times for increasingly filtrating the FS molecules (g and h). Eventually, after a total of 96 h of dialysis, the FS molecules are fully filtrated, producing negligible fluorescence for the right-hand sample; in comparison, the as-prepared SiNPs are still retained due to their relatively larger sizes, exhibiting stable and bright fluorescence (i).

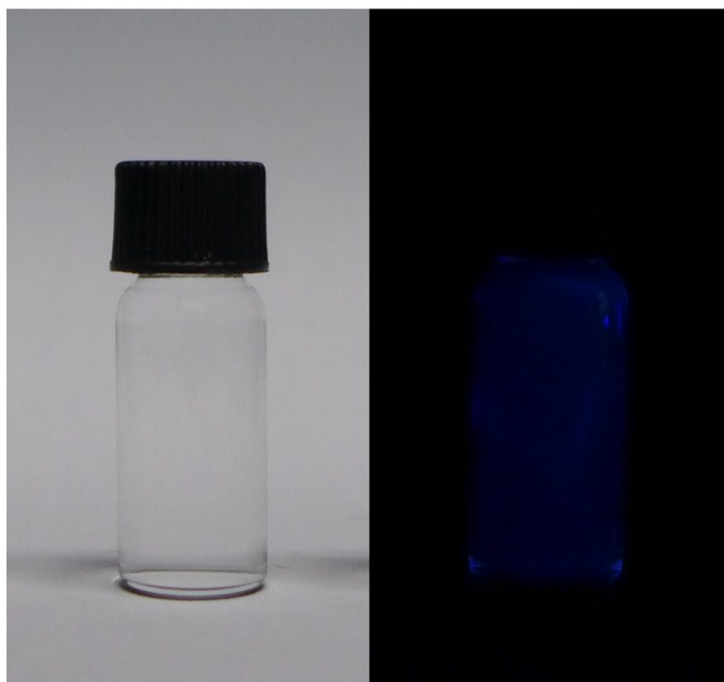


Fig. S15 Photographs of the APS (after microwave reaction) under ambient light (left) and 365 nm irradiation right. As shown in Fig. S15, after 180 °C/ 1h treatment with microwave irradiation, the aqueous solution of APS shows extremely feeble blue luminescence under UV irradiation.

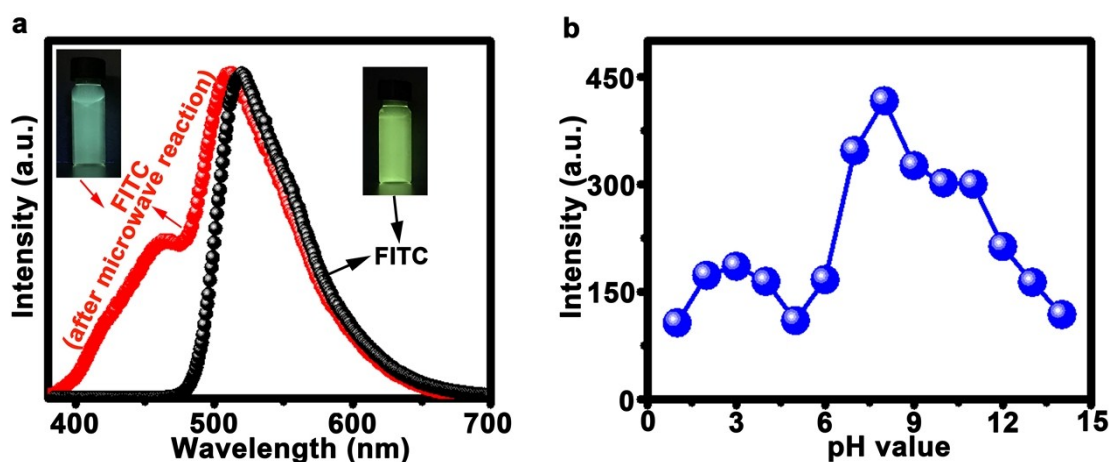


Fig. S16 (a) Photoluminescence spectra and photograph of FITC without microwave treatment and FITC (after microwave reaction). (b) Temporal evolution of fluorescence intensity of FITC aqueous sample solution under various pH values. Fig. S16a presents the normalized PL spectra of FITC without microwave treatment and FITC (after microwave reaction), indicating the maximum emission wavelength of FITC without microwave treatment and FITC (after microwave reaction) locate at 520 nm, and 515 nm, respectively. In comparison to FITC without microwave treatment, the PL spectra of the FITC (after microwave reaction) exhibits a shoulder peak, which can be attributable to degradation of FITC under microwave irradiation. The aqueous solution of FITC without microwave treatment and FITC (after microwave reaction) show distinct green-emitting luminescence and blue-green luminescence under UV irradiation (Fig. S16a, inset), respectively. Furthermore, we study the pH stability of FITC (after microwave reaction). As displayed in Fig. S16b, FITC (after microwave reaction) in water exhibits inferior pH stability. The PL intensity of FITC (after microwave reaction) severely decreases for pH values less than 8, and vice versa. Specifically, the PL intensity of FITC (after microwave reaction) decreases by ~75% in acidic-to-basic environments in the pH range of 1-14.

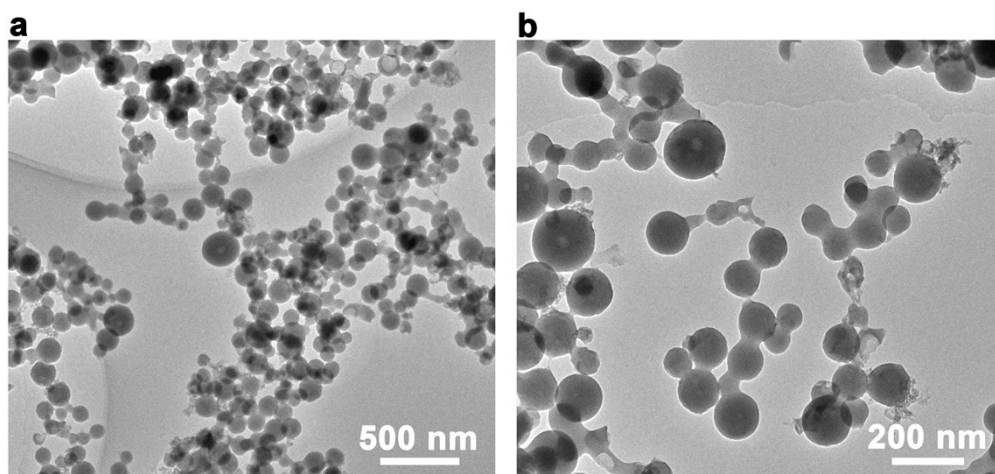


Fig. S17 (a) and (b) TEM images of the SiO₂. As shown in Fig. S17, the as-prepared SiO₂ appear as spherical particles, and have relative small sizes with around 120 nm.

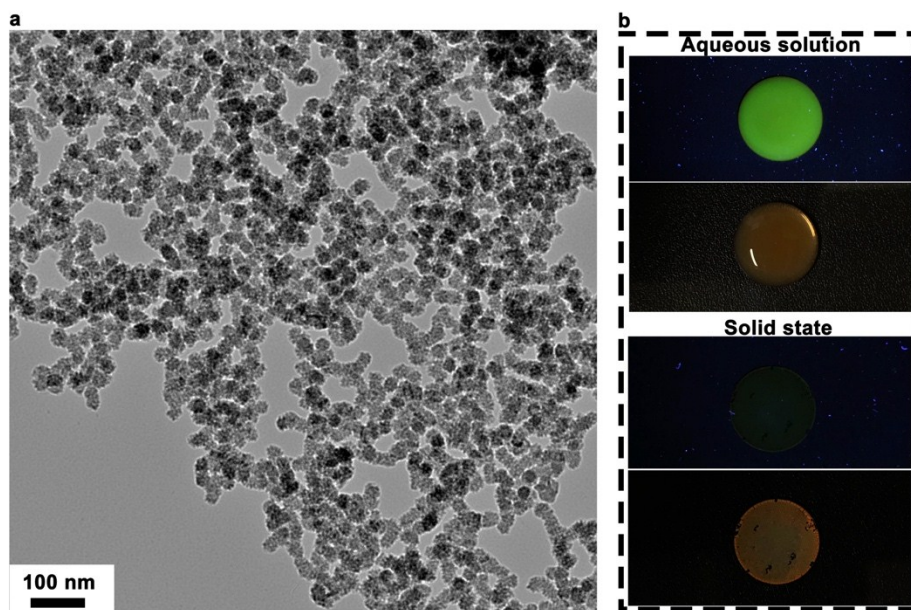


Fig. S18 (a) TEM image of SiO_2 with small size of ~ 20 nm. (b) Photographs of $\text{SiO}_2@$ FS (~ 20 nm SiO_2) sample under ambient light or 365 nm irradiation. As shown in Fig. S18, the aqueous solution of the $\text{SiO}_2@$ FS exhibits green luminescence under UV irradiation (Aqueous solution - top). However, the solid-state sample of the $\text{SiO}_2@$ FS exhibits feeble fluorescence under UV irradiation (Solid state - top). While the $\text{SiO}_2@$ FS have different sizes (e.g., ~ 120 nm and ~ 20 nm), they show similar optical properties in the solid state, suggesting that the sizes of SiO_2 have little influence on the optical properties of FS molecules.

Table S1. A comparison chart of different SiNPs synthesis methods

	The top-down strategy		The bottom-up strategy			Others	Surface modification of SiNPs	
	Electrochemical/chemical etching of bulk silicon	Breakdown of silicon rich oxides	Solution-phase reduction of silicon halides	Utilization of silicon Zintl salts (ASi _x , A= Na, K, Mg, etc.) to prepare silicon nanocrystals	To synthesize SiNPs in aqueous phase by using organosilicon as silicon source			
Representative literatures	Appl. Phys. Lett. 2002, 80, 841-843; J. Am. Chem. Soc. 2007, 129, 5326-5327; Adv. Mater. 2009, 21, 661-664; Chem. Commun. 2009, 3759-3761; etc.	Chem. Mater. 2006, 18, 637-642; Langmuir 2005, 21, 6324-6329; Chem. Mater. 2006, 18, 6139-6146; J. Phys. Chem. C 2007, 111, 6956-6961; Adv. Mater. 2007, 19, 3513-3516; Chem. Mater. 2012, 24, 393-401; etc.	Chem. Commun. 2002, 1822-1823; Angew. Chem. Int. Ed. 2005, 44, 4550-4554; J. Am. Chem. Soc. 2010, 132, 248-253; Nanoscale 2011, 3, 3364-3370; Chem. Commun. 2011, 47, 4941-4943; Chem. Commun. 2012, 48, 11874-11876; etc.	J. Am. Chem. Soc. 1999, 121, 5191-5195; Chem. Mater. 2001, 13, 765-770; Nano Lett. 2004, 4, 1181-1186; Chem. Mater. 2011, 23, 2407-2418; etc.	J. Am. Chem. Soc. 2013, 135, 8350-8356; ACS Nano 2015, 9, 5958-5967; Chem. Commun. 2005, 2016, 52, 13444-13447; Adv. Mater. Interfaces 2-15, 2, 150036; ACS Appl. Mater. Interfaces 2018, 10, 27979-27986; Anal. Chem. 2017, 89, 3001-3008; Anal. Chem. 2016-88, 9789-9795; etc.	J. Am. Chem. Soc. 2001, 123, 3743-3728; Appl. Phys. Lett. 2006, 88, 233116; Chem. Mater. 1998, 10, 3278-3281; ACS Nano 2013, 7, 7303-7310; J. Am. Chem. Soc. 2011, 133, 14192-14195; J. Am. Chem. Soc. 2015, 137, 14726-14732; etc.	J. Am. Chem. Soc. 2013, 135, 14924-14927; ACS Nano 2013, 7, 2676-2685; ACS Nano 2014, 8, 9636-9648; Light: Sci. & Appl. 2015, 4, e245; J. Mater. Chem. B 2014, 2, 8427-8433; ACS Nano 2016, 10, 8385-8393; etc.	This work
Morphology	Nanoparticles (diameter: ~1.0-4.0 nm)	Nanoparticles (diameter: ~2-16 nm)	Nanoparticles (diameter: ~1.5-10 nm)	Nanoparticles (diameter: ~2-5.7 nm)	Nanoparticles (diameter: ~2-5 nm)	Nanoparticles (diameter: ~2-5 nm)	Nanoparticles (diameter: ~2.4-6 nm)	Nanoparticles (diameter: ~3.7-5.3 nm)
Spectral properties: (1) The maximum emission wavelength; (2) Luminescent color; (3) full width at half-maximum (FWHM)	(1) The maximum emission wavelength: ~400-780 nm; (2) Luminescent color: from blue to Near-IR; (3) FWHM: ~60-100 nm.	(1) The maximum emission wavelength: ~390-1060 nm; (2) Luminescent color: from UV to Near-IR; (3) FWHM: ~15-200 nm.	(1) The maximum emission wavelength: ~320-480 nm; (2) Luminescent color: blue (3) FWHM: ~70-120 nm	(1) The maximum emission wavelength: ~350-550 nm; (2) Luminescent color: from UV-blue to blue-green (3) FWHM: ~70-110 nm	(1) The maximum emission wavelength: 430-600 nm; (2) Luminescent color: blue to orange (3) FWHM: ~70-100 nm	(1) The maximum emission wavelength: ~420-800 nm; (2) Luminescent color: from blue to Near-IR; (3) FWHM: ~30-120 nm	(1) The maximum emission wavelength: ~410-730 nm; (2) Luminescent color: from blue to Near-IR; (3) FWHM: ~40-100 nm	(1) The maximum emission wavelength: ~515 nm; (2) Luminescent color: green (3) FWHM: ~50 nm
Photoluminescent quantum yield (PLQY)	~0.4-10%		~0.9-25%		~5-80%	~1.8-60%	12-90%	~90%

References

- 1 (a) Y. L. Zhong, F. Peng, F. Bao, S. Y. Wang, X. Y. Ji, L. Yang, Y. Y. Su, S. T. Lee and Y. He, *J. Am. Chem. Soc.*, 2013, **135**, 8350-8356; (b) L. Yang, Y. Liu, Y. L. Zhong, X. X. Jiang, B. Song, X. Y. Ji, Y. Y. Su, L. S. Liao and Y. He, *Appl. Phys. Lett.*, 2015, **106**, 173109; (c) Y. L. Zhong, B. Song, F. Peng, Y. Y. Wu, S. C. Wu, Y. Y. Su and Y. He, *Chem. Commun.* 2016, **52**, 13444-13447.
- 2 (a) Y. W. Liu, J. Bai, X. D. Jia, X. Jiang and Z. Guo, *ACS Appl. Mater. Interfaces*, 2015, **7**, 112-121; (b) K. Ma, H. Sai and U. Wiesner, *J. Am. Chem. Soc.*, 2012, **134**, 13180-13183.
- 3 S. C. Wu, Y. L. Zhong, Y. F. Zhou, B. Song, B. B. Chu, X. Y. Ji, Y. Y. Wu, Y. Y. Su and Y. He, *J. Am. Chem. Soc.*, 2015, **137**, 14726-14732.
- 4 Y. He, Y. L. Zhong, F. Peng, X. P. Wei, Y. Y. Su, Y. M. Lu, S. Su, W. Gu, L. S. Liao and S. T. Lee, *J. Am. Chem. Soc.*, 2011, **133**, 14192-14195.
- 5 Y. L. Zhong, F. Peng, X. P. Wei, Y. F. Zhou, J. Wang, X. X. Jiang, Y. Y. Su, S. Su, S. T. Lee and Y. He, *Angew. Chem. Int. Ed.*, 2012, **51**, 8485-8489.
- 6 Y. L. Zhong, X. T. Sun, S. Y. Wang, F. Peng, F. Bao, Y. Y. Su, Y. Y. Li, S. T. Lee and Y. He, *ACS Nano*, 2015, **9**, 5958-5967.
- 7 Y. He, Y. Y. Su, X. B. Yang, Z. H. Kang, T. T. Xu, R. Q. Zhang, C. H. Fan and S. T. Lee, *J. Am. Chem. Soc.*, 2009, **131**, 4434-4438.
- 8 Y. He, L. M. Sai, H. T. Lu, M. Hu, W. Y. Lai, Q. L. Fan, L. H. Wang and W. Huang, *Chem. Mater.*, 2007, **19**, 359-365.
- 9 Y. He, Y. L. Zhong, Y. Y. Su, Y. M. Lu, Z. Y. Jiang, F. Peng, T. T. Xu, S. Su, Q. Huang, C. H. Fan and S. T. Lee, *Angew. Chem. Int. Ed.*, 2011, **50**, 5695-5698.
- 10 M. M. Martin and L. Lindqvist, *J. Lumin.*, 1975, **10**, 381-390.
- 11 G. Weber and F. W. J. Teale, *Trans. Faraday Soc.*, 1958, **54**, 640-648.

- 12 M. Dasog, G. B. De los Reyes, L. V. Titova, F. A. Hegmann and J. G. C. Veinot, *ACS Nano*, 2014, **8**, 9636-9648.
- 13 M. Dasog, J. Kehrle, B. Rieger and J. G. C. Veinot, *Angew. Chem. Int. Ed.*, 2015, **54**, 2-20.
- 14 Q. Li, T. Y. Luo, M. Zhou, H. Abroshan, J. C. Huang, H. J. Kim, N. L. Posi, Z. Z. Shao and R. C. Jin, *ACS Nano*, 2016, **10**, 8385-8393.
- 15 D. D. Jiang, Q. Yao, M. A. Mckinney and C. A. Wilkie, *Polym. Degrad. Stabil.*, 1999, **63**, 423-434.
- 16 K. P. Reis, A. Ramanan and M. S. Whittingham, *Chem. Mater.*, 1990, **2**, 219-221.
- 17 Y. Y. Wu, Y. L. Zhong, B. B. Chu, B. Sun, B. Song, S. C. Wu, Y. Y. Su, Y. He, *Chem. Commun.*, 2016, **52**, 7047-7050.
- 18 B. Song, Y. L. Zhong, H. Y. Wang, Y. Y. Su and Y. He, *Chem. Commun.*, 2017, **53**, 6957-6960.
- 19 B. Song, Y. L. Zhong, S. C. Wu, B. B. Chu, Y. Y. Su and Y. He, *J. Am. Chem. Soc.*, 2016, **138**, 4824-4831.
- 20 L. L. Wang, A. Roitberg, C. Meuse and A. K. Gaigalas, *Spectrochim. Acta, Part A*, 2001, **57**, 1781-1791.
- 21 M. Davies and R. L. Jones, *J. Chem. Soc.*, 1954, 120-125.
- 22 Y. Yoon, B. Lee, K. S. Lee, G. H. Im, S. Byeon, J. H. Lee and I. S. Lee, *Adv. Funct. Mater.*, 2009, **19**, 3375-3380.
- 23 F. J. Hua, M. T. Swihart and E. Ruckenstein, *Langmuir*, 2005, **21**, 6054-6062.
- 24 T. K. Purkait, M. Iqbal, M. H. Wahl, K. Gottschling, C. M. Gonzalez, M. A. Islam and G. C. Veinot, *J. Am. Chem. Soc.*, 2014, **136**, 17914-17917.
- 25 J. Zou, R. K. Baldwin, K. A. Pettigrew and S. M. Kauzlarich, *Nano Lett.*, 2004, **4**, 1181-1186.

- 26 N. I. Hammer, K. T. Early, K. Sill, M. Y. Odoi, T. Emrick and M. D. Barnes, *J. Phys. Chem. B*, 2006, **110**, 14167-14171.
- 27 M. Y. Odoi, N. I. Hammer, K. Sill, T. Emrick and M. D. Barnes, *J. Am. Chem. Soc.*, 2006, **128**, 3506-3507.
- 28 B. K. An, S. K. Kwon, S. D. Jung and S. Y. Park, *J. Am. Chem. Soc.*, 2002, **124**, 14410-14415.
- 29 M. G. Liu, M. H. Jia, H. F. Pan, L. Li, M. F. Chang, H. Ren, F. Argoul, S. J. Zhang and J. H. Xu, *Appl. Spectrosc.*, 2014, **68**, 577-583.
- 30 Y. Zhou, Y. Xiao, S. M. Chi and X. H. Qian, *Org. Lett.*, 2008, **10**, 633-636.
- 31 A. Hepp, G. Ulrich, R. Schmechel, H. V. Seggern and R. Ziessel, *Synth. Met.*, 2004, **146**, 11-15.
- 32 W. K. Walthall and J. D. Srark, *Environ. Pollut.*, 1999, **104**, 207-215.
- 33 N. Nakayama-Ratchford, S. Bangsaruntip, X. M. Sun, K. Welsher and H. J. Dai, *J. Am. Chem. Soc.*, 2007, **129**, 2448-2449.
- 34 H. Diehl and R. Markuszewski, *Talanta*, 1989, **36**, 416-418.
- 35 T. K. Purkait, M. Iqbal, M. A. Islam, M. H. Mobarok, C. M. Gonzalez, L. Hadidi and J. G. C. Veinot, *J. Am. Chem. Soc.*, 2016, **138**, 7114-7120.
- 36 R. J. Anthony, K. Y. Cheng, Z. C. Holman, R. J. Holmes and U. R. Kortshagen, *Nano Lett.*, 2012, **12**, 2822-2825.
- 37 J. H. Warner, A. Hoshino, K. Yamamoto and R. D. Tilley, *Angew. Chem. Int. Ed.*, 2005, **44**, 4550-4554.
- 38 B. Kopainsky, P. Qiu and W. Kaiser, *Appl. Phys. B*, 1982, **29**, 15-18.